JMEPEG (2005) 14:604-609
DOI: 10.1361/105994905X66015

1059-9495/$19.00

Casting/Mold Thermal Contact Heat Transfer during Solidification of Al-Cu-Si Alloy (LM 21) Plates in Thick and Thin Molds

K. Narayan Prabhu, Bheemappa Chowdary, and N. Venkataraman

(Submitted June 16, 2003; in revised form August 4, 2005)

Heat flow at the casting/mold interface was assessed and studied during solidification of Al-Cu-Si (LM 21) alloy in preheated cast iron molds of two different thicknesses, coated with graphite and alumina based dressings. The casting and the mold were instrumented with thermocouples connected to a computer controlled temperature data acquisition system. The thermal history at nodal locations in the mold and casting obtained during experimentation was used to estimate the heat flux by solving the one-dimensional inverse heat conduction problem. The cooling rate and solidification time were measured using the computer-aided cooling curve analysis data. The estimated heat flux transients showed a peak due to the formation of a stable solid shell, which has a higher thermal conductivity compared with the liquid metal in contact with the mold wall prior to the occurrence of the peak. The high values of heat flux transients obtained with thin molds were attributed to mold distortion due to thermal stresses. For thin molds, assumption of Newtonian heating yielded reliable interfacial heat transfer coefficients as compared with one-dimensional inverse modeling. The time of occurrence of peak heat flux increased with a decrease in the mold wall thickness and increase in the casting thickness.

Keywords casting/mold interface, heat conduction, inverse modeling, Newtonian heating, solidification

1. Introduction

The success of simulation-based process design of castings to predict accurately the thermal history and to locate hot spots inside the casting depends to a large extent on a reliable database on the heat transfer boundary conditions specified at the casting/mold interface (Ref 1-4). Further, when the metal and the mold have good rates of conductance, the boundary between the two becomes the region of dominant resistance (Ref 5).

A perfect contact between the metal and the mold surfaces may not be realized in actual practice as the surface irregularities of the solidifying skin results in irregular contacts to be established between the die-wall and the skin. The degree of thermal resistance at the interface is a function of actual contact area, thermal and physical properties of the materials in contact, and interstitial fluid present in the voids formed by the two contacting surfaces (Ref 6, 7). The thermal resistance to heat transfer results in a temperature drop at the interface. The heat transfer at the interface can be characterized either by interfacial heat flux q or by an interfacial heat transfer coefficient h, defined as the ratio of the interfacial heat flux to the temperature drop at the interface. Mathematically h is expressed as: $h = q/\Delta T$.

When conditions are favorable, a skin of solidifying casting may physically separate from the mold wall resulting in a gap of finite thickness. The mold configuration and Biot number have been shown to be important parameters affecting the formation of the gap (Ref 8). Once the air gap forms, the heat transfer across the interface drops rapidly. Conduction is the predominant mode of heat transfer through the gap at lower temperatures. While the radiation heat transfer depends on the surface temperatures and emissivities, conduction heat transfer depends on the thermal conductivity of the gas in the gap and the air gap size as well. The heat transfer coefficients due to radiation (h_r) and conduction (h_c) are expressed as:

$$h_r = \frac{(T_c^2 + T_m^2)(T_c + T_m)}{\frac{1}{\varepsilon_c} + \frac{1}{\varepsilon_m} - 1}$$

$$h_c = \frac{k_g}{\delta}$$

T_c and T_m are the casting surface and mold surface temperatures, respectively; ε_c and ε_r are the emissivities of the casting and mold surfaces; and k_g and δ are the thermal conductivity of the gas in the gap and the width of the gas gap, respectively. Complexities of material behavior, metallostatic pressure, and mold geometry make the calculation of air gap formation very difficult. Further, the air gap does not start simultaneously at all points in the casting and the magnitude of the air gap continuously varies with time (Ref 9, 10). Gravity die-casting, pressure die-casting, investment casting, continuous casting, and twin-roll casting are some of the processes where the product quality

K. Narayan Prabhu, Department of Metallurgical & Materials Engineering, National Institute of Technology Karnataka, Surathkal, P.O. Srinivasnagar 575 025, India; **Bheemappa Chowdary,** Formerly Graduate Student, NITK, Surathkal, and now with M/s Chowgule Industries Limited, Panaji, Goa, India; and **N. Venkataraman,** Professor (Retd.), National Institute of Technology Karnataka, Surathkal, India. Contact e-mail: prabhukn_2002@yahoo.co.in.

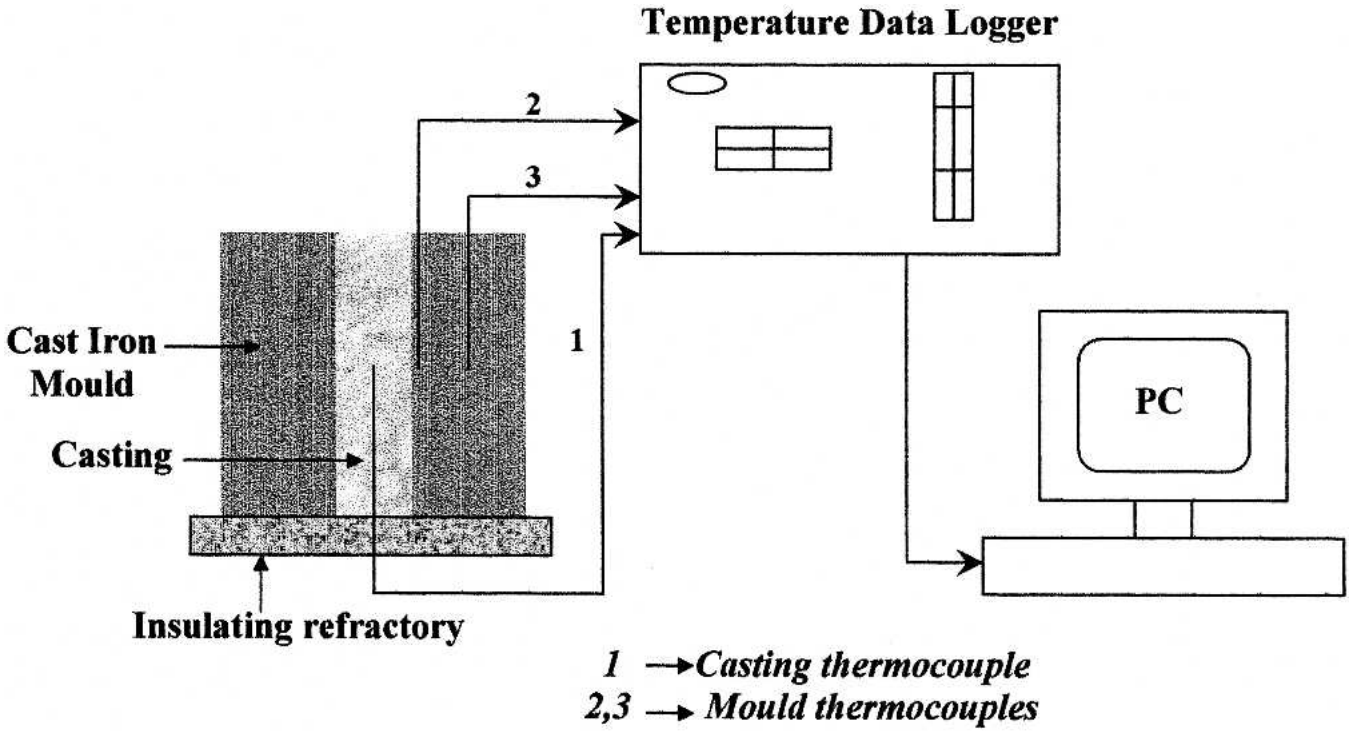

Fig. 1 Schematic sketch of the experimental setup

is affected by interfacial heat transfer conditions (Ref 11-14). The quantification of heat transfer across the interface depends on the knowledge of many factors like interface temperatures, thermal properties of the gas in the gap, surface texture of the mold surface, coating material and composition, etc. (Ref 15-17). Modeling of the casting/mold interfacial heat transfer is, thus, one of the critical problems in numerical simulation of casting solidification.

In the present work, thermal contact heat transfer at the interface between plate type castings of Al-Cu-Si alloy (LM 21), solidifying in thick and thin cast iron molds, was assessed and investigated.

2. Experimental Method

Cast iron mold halves of thicknesses 10 and 38 mm were fabricated to cast aluminum alloy plates of dimensions 100 × 70 × 12 mm and 100 × 70 × 22 mm. Figure 1 shows a schematic diagram of the experimental setup. Two K-type thermocouples (2 and 3) of 0.45 mm diameter were introduced at different nodal locations inside the mold. For the 10 mm mold, thermocouples 2 and 3 were located at 2 and 6 mm from the mold surface in contact with the casting. The corresponding locations for the 38 mm mold were at 2 and 26 mm, respectively. The geometric center of the casting was also instrumented with a similar thermocouple (1) to monitor the solidification of the casting. The thermocouples were connected by means of compensating cables to a temperature data logger. All the experiments were carried out with a coating on the inner surface of the mold. The mold halves were heated to about 180 °C and coating material was sprayed on their surface to a thickness of 100 μm using a spray gun. Alumina and graphite based die coats were used for this purpose. Table 1 gives the composition of the coating materials used. The molds were preheated to 100 °C prior to pouring of castings.

Table 1 Composition of mold dressings

Coating type	Composition, wt.%			
	Alumina	Graphite	Sodium silicate	Water
1	17	…	11	72
2	…	16	4	80

LM 21 alloy ingots were melted in an electric resistance furnace. Table 2 gives the composition of the alloy. The pouring temperature was maintained at around 700 °C. The data logger was activated a few seconds before pouring. After experimentation, the thermocouple signals stored in the temperature data logger were transferred to a computer by an off-line procedure. Table 3 gives the thermophysical properties of the alloy and the cast iron mold material.

Beck's nonlinear estimation technique (Ref 18) was used to estimate the mold surface heat flux from knowledge of measured thermal history at nodal locations inside the mold. The one dimensional heat conduction equation:

$$\frac{\partial}{\partial x}\left(k\frac{\partial T}{\partial x}\right)=\rho c_p\left(\frac{\partial T}{\partial t}\right) \quad \text{(Eq 1)}$$

was solved inversely subject to the following boundary and initial conditions.

$$T(2, t) = Y(t)$$

$$T(3, t) = B(t)$$

$$T(x, 0) = T_i(x)$$

Table 2 Composition (wt.%) of the Al-Cu-Si alloy (LM21)

Si	Cu	Ni	Zn	Fe	Mg	Ca	Na	Ti	Al
5.6	3.07	0.31	2.02	0.47	0.47	0.0028	0.0011	0.02	balance

Table 3 Thermophysical properties of the mold material and casting alloy

Material	Density, kg/m^3	Thermal conductivity, W/m · K	Specific heat, J/kg · K
Mold:			
Cast iron	7200	72	502
Casting:			
LM21 alloy			
Liquid	2560	90	1254
Solid	2690	194	1164

To find the heat flux at the casting/mold interface, the following function based on a least squares analysis was minimized.

$$F(q) = \sum_{i=1}^{I=mr} (T_{\eta+i} - Y_{\eta+i})^2 \quad \text{(Eq 2)}$$

The variable r is the number of future time temperatures +1, and m is the $\Delta\theta/\Delta t$. $\Delta\theta$ and Δt are the time steps for heat flux and temperature, respectively. Y_{n+i} and T_{n+i} are the measured and calculated temperatures, respectively, at the temperature node (TC1) located in the mold near to the casting/mold interface. The future temperatures are the calculated temperatures at time steps greater than the present time steps estimated using the measured temperatures at location TC3 as the known boundary condition. The unknown heat flux $q(0,t)$ was approximated by some arbitrary value in the initial time step.

Minimizing Eq 2 with respect to q, by setting the partial derivative to zero, the correction term for heat flux was obtained as:

$$\nabla q_{M+1}^{1} = \frac{\sum_{i=1}^{I} (Y_{n+i} - T_{n+i}^{l-1}) \phi_i^{l-1}}{\sum_{i=1}^{I} (\phi_i^{l-1})^2} \quad \text{(Eq 3)}$$

where $\nabla q_{M+1}{}^{1} = q_{M+1}{}^{1} - q_{M+1}{}^{l-1}$.

The procedure was then repeated for a new heat flux value. The iteration was continued until:

$$\frac{\nabla q_{M+1}^{l}}{q_{M+1}^{l-1}} < 0.005 \quad \text{(Eq 4)}$$

the final iterated value of q was used as the initial heat flux for estimating the heat flux for the next time step. The calculation of the heat flux was continued for the desired time period.

The partial derivative in Eq 3 is called the sensitivity coefficient and is a measure of the change in the estimated temperatures with a small change in the boundary condition.

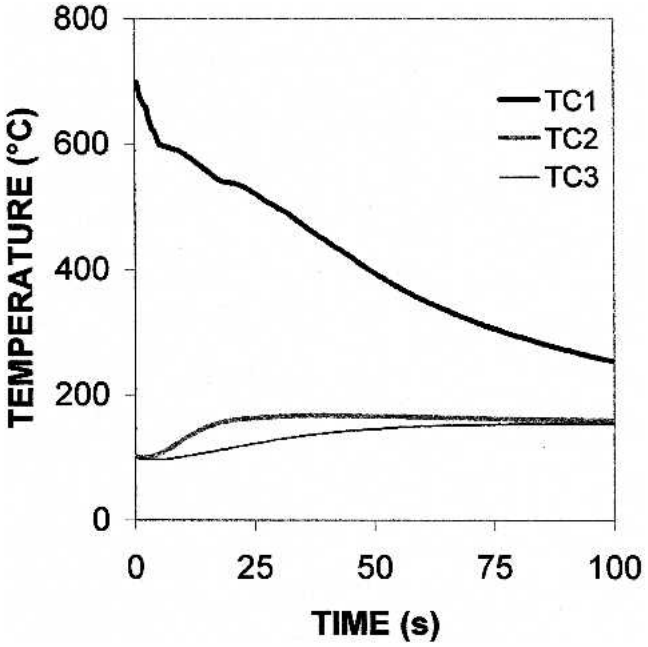

Fig. 2 Casting and mold thermal history during solidification of 12 mm thick casting in a 38 mm thick graphite coated mold

It was calculated by using Eq 4:

$$\phi_i^{l-1} = \frac{T_{n+i}[q_{M+1}^{l-1}(1+\varepsilon)] - T_{n+i}(q_{M+1}^{l-1})}{\varepsilon q_{M+1}^{l-1}} \quad \text{(Eq 5)}$$

where the numerator is the difference in temperatures calculated using an explicit finite difference scheme at the monitored node at the same time step for temperature (ΔT), using the boundary conditions q and $q + \varepsilon$. ε is a small number and was taken as 0.001 in the present investigation.

3. Results and Discussion

Figures 2 and 3 show the typical thermal histories in the casting and the mold during solidification of the alloy in the mold coated with graphite based dressing. The liquid metal cools rapidly from the pouring temperature to the liquidus temperature. At the liquidus and solidus temperatures, the cooling curve shows a rapid change in the slope due to the evolution of the latent heat. It is also observed that during solidification of the alloy the locations in the mold near the mold surface in contact with the solidifying casting heated rapidly to the maximum temperature.

Analysis of casting and the mold thermal history indicated the following:

- The peak temperature attained by the mold during solidification increased with a decrease in the mold wall thickness. This is attributed to the lower volumetric heat capacity ($\rho C_p V$) of the thin walled molds.
- The peak mold temperature increased with an increase in the casting thickness due to its higher heat content.
- The change in the coating material had a significant effect

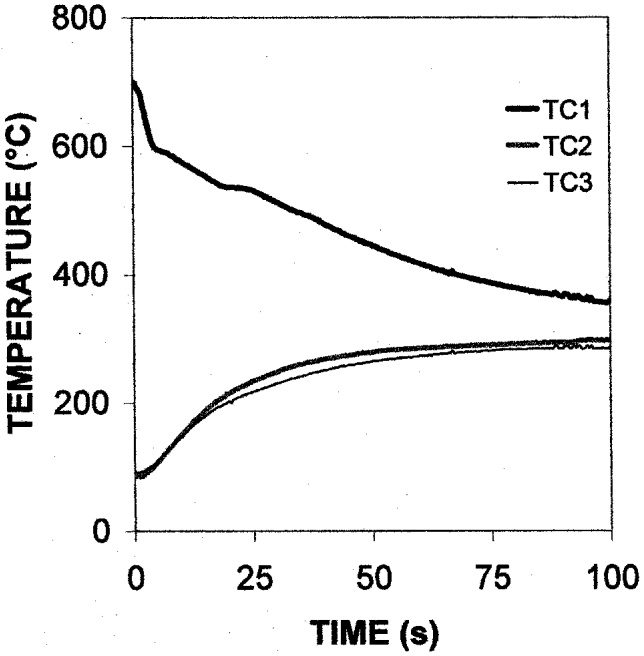

Fig. 3 Casting and mold thermal history during solidification of 12 mm thick casting in a 10 mm thick graphite coated mold

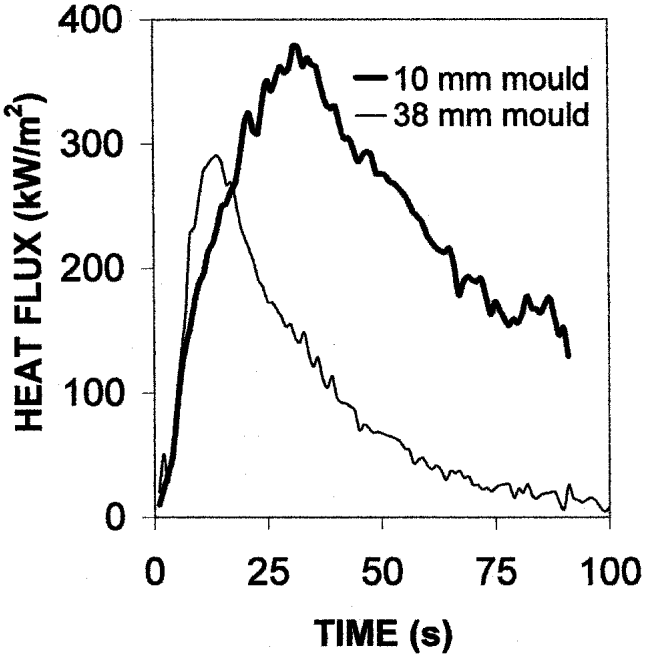

Fig. 4 Estimated heat flux transients for 12 mm thick casting solidifying in graphite coated molds

on mold thermal history. The molds coated with the graphite-based mold wash exhibited higher temperatures compared with those coated with the alumina based mold coat.

Figures 4 and 5 show the computed heat flux transients for typical casting/mold combinations. As the liquid metal filled the mold, superheat is dissipated from the liquid metal to the casting. This is shown in the cooling curve as a rapid decrease in casting temperature. Below the liquidus temperature a solid skin is formed. The casting skin may be pushed against the mold wall by the metallostatic pressure of the liquid metal resulting in a conforming contact. The good contact at the casting/mold interface increases heat transfer from the solidifying casting to the mold, which causes a drop in the casting skin temperature. The peak in the heat flux transient can be associated with the formation of a stable shell at the casting/mold interface.

The initial heat flux transients were low for all of the experiments. It is expected that the true heat flux begins at a high value and then declines with time. One of the methods adopted to approximate the true value of the peak heat flux is to extrapolate the heat flux transient curve at the point of peak heat flux to meet the ordinate at zero time. However, due to the asymptotic nature of the curve it results in very high values of the peak heat flux to be justified by the type of experiment. Further, the peak in the heat flux transient curve is always identified with the solidification of the casting surface in contact with the chill. For the aluminum alloy LM21, the thermal conductivity of the solid (k_{solid} = 194 W/m · K) is more than twice the thermal conductivity of liquid (k_{liquid} = 90 W/m · K). Hence, the heat flux at the point of casting skin solidification is greater than the heat flux at the liquid metal/chill interface. An increase in the heat flux is, therefore, expected during the formation of a stable solidified shell.

As the thickness of the solidified shell increases, its strength increases, which can resist the metallostatic pressure, allowing possible contraction away from the mold wall. This could result in a nonconforming contact in the casting/mold interfacial region causing a sharp decrease in the heat flux transients. If the conditions are favorable, a gas gap may form at the interface. The formation of the gas gap during solidification of an aluminum alloy against a metallic chill has been experimentally proved by Prabhu and Campbell using real-time x-ray imaging (Ref 19).

The graphite coated molds showed higher heat flux transients compared with that obtained with alumina-coated molds. This is due to the higher thermal conductivity of the graphite-based mold coats. It was also observed that the 10 mm thick mold resulted in high heat flux transients and the heat flow was found to be higher compared with 38 mm thick molds. On the contrary, the solidification time and the cooling rates increased with increase in the mold wall thickness. A similar result was observed by Prabhu and Campbell (Ref 19) during solidification of an aluminum alloy against metallic chills. Copper and cast iron chills of 10 mm thickness appeared to show abnormally high values of heat transfer coefficients. It was inferred that the thin 10 mm chills, being relatively flexible, expand as their front face heats up on contact with the solidifying casting. The improved contact will cause the front face to heat up further, enhancing the distortion toward the casting. On the other hand, the thick chills, having greater rigidity, keep their shape and location while the casting contracted, leading to a nonconforming contact/gas gap. It is also likely that the heat transfer might not be truly unidirectional and one-dimensional inverse analysis may not be applicable in the case of thin chills/molds. In light of contradicting results obtained with thin molds, it is necessary to reassess the heat transfer at the casting/thin mold wall interface.

In the present investigation, for thin molds, the thermal histories at all locations inside the mold wall were approximated by a single mold heating curve determined by taking the mean of the temperatures at two different locations (2 and 3)

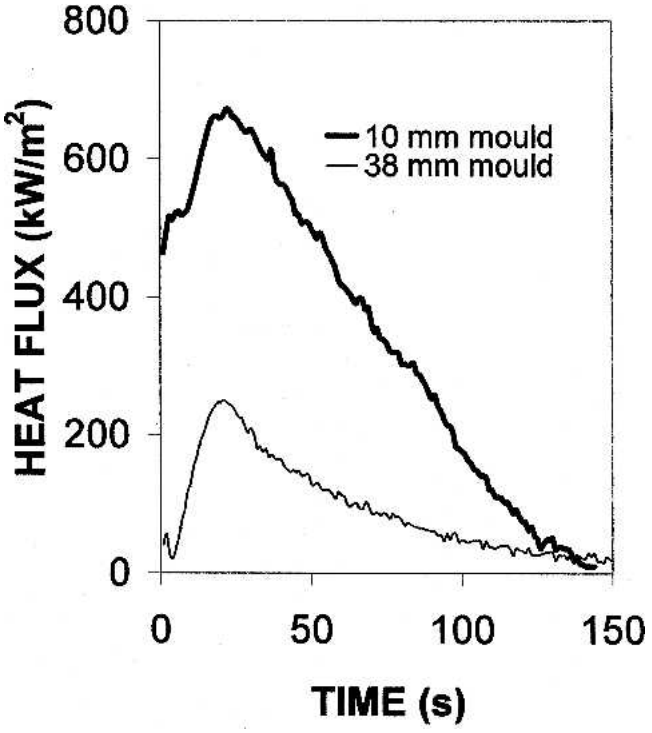

Fig. 5 Estimated heat flux transients for 12 mm thick casting solidifying in alumina coated molds

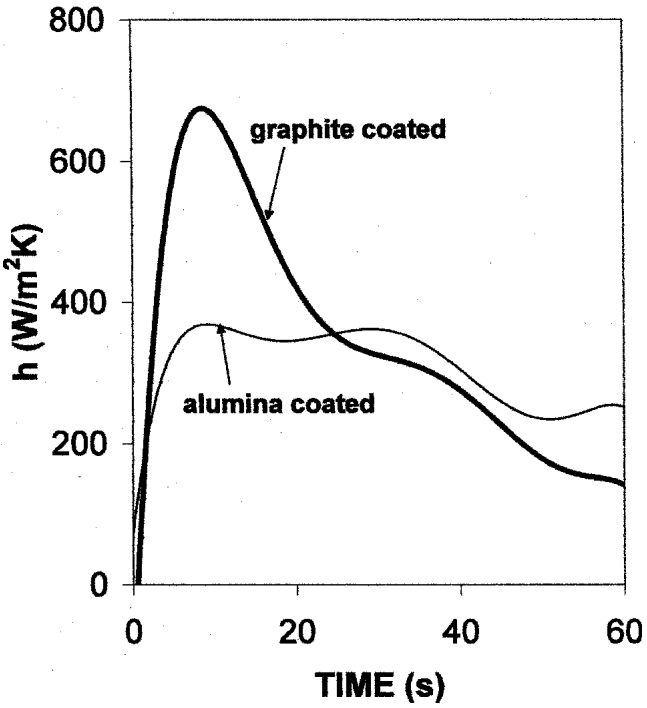

Fig. 6 Heat transfer coefficients estimated assuming Newtonian heating for 10 mm thick molds

inside the mold. The casting/mold interfacial heat transfer coefficients were then estimated by adopting Newtonian heating analysis. The following equation is used to estimate the heat transfer coefficient for 10 mm molds.

$$h = \frac{\rho V C_p \dfrac{\partial T}{\partial t}}{A(T_c - T_m)} \qquad \text{(Eq 6)}$$

ρ, C_p, and V/A are the density, specific heat, and volume-to-surface area ratio of the mold, respectively. T_m is the mold temperature obtained as the mean of the temperatures at mold locations 2 and 3. $\partial T/\partial t$ is the heating rate of the mold calculated by taking the derivative of the heating curve $T_m(t)$. T_c is the casting temperature measured at location TC1.

Figure 6 shows the interfacial heat transfer coefficients estimated using Newtonian heating for the alloy solidifying against 10 mm thick molds coated with graphite- and alumina-based dressings. The peak heat transfer coefficient was nearly 700 W/m^{2}K for the graphite-coated mold. The corresponding mold temperature was 162 °C. Assuming the peak to be associated with the formation of solid shell, the peak flux at this point was calculated as:

$$Q/A = q = h\,(T_{solidus} - T_m) = 700\,(525 - 162) = 254{,}100\ W/m^2 = 254.1\ kW/m^2$$

This value is significantly less compared with the peak heat flux (380 kW/m^2) obtained by inverse analysis for the mold of same thickness and also the peak heat flux estimated for the thick mold. Further, the Biot number corresponding to the peak heat transfer coefficient is calculated as:

$$\text{Bi} = \frac{hl}{k} = \frac{(700)(0.01)}{72} = 0.0972$$

The corresponding peak heat flux and the Biot number for the alumina-coated mold are found to be 154 kW/m^2 and 0.055, respectively. In both cases, the Biot number is less than 0.1 indicating that in 10 mm thick molds, the temperature at the surface of the mold in contact with the solidifying casting did not differ greatly from the temperature at the center by more than 5%. Hence, the assumption of a uniform temperature for the 10 mm mold is valid. The heat transfer boundary conditions calculated by using Newtonian heating analysis seem to be more reliable as compared with the heat flux transients estimated by inverse analysis for thin molds. However, the Newtonian heating analysis cannot be applied for thick molds where the Biot number is greater than 0.1 due the higher thermal resistance (l/k) offered by the mold.

It was also observed that the time for the occurrence of peak heat flux increased with the decrease in mold wall thickness and increase in casting thickness. For example, the increase in the casting thickness from 12 to 22 mm resulted in an increase in the time of occurrence of the peak value from 16 to 21 s. With a decrease in mold wall thickness, the ability to extract heat from the casting decreases. The solidifying metal at the interface remains a liquid for a longer time. With an increase in mold wall thickness, a solid shell of the metal forms early at the interface, corresponding to the peak in the heat flux transients, and as the solidified shell gains strength it contracts away from the mold wall. Similarly, with an increase in casting thickness the total heat content of the casting to be extracted by the mold of similar thickness increases, leading to a delay in the formation of the solid shell at the casting/mold interface.

4. Conclusions

Based on the preceding results and discussion the following conclusions were drawn:

- The mold wall, casting thicknesses, and the coating material of the mold significantly affect the thermal behavior of the mold, and hence, the solidification of the casting.
- The interfacial heat flux transients (q) estimated by inverse analysis were found to be higher for thin molds, although the solidification times were lower. The contradictory results obtained with thin molds were attributed to mold distortion due to thermal stresses.
- For thin metallic molds, where the Biot number is small, assumption of Newtonian heating yielded realistic and reliable assessment of the casting/mold interfacial heat transfer compared with one-dimensional inverse modeling.
- The time of occurrence of peak heat flux associated with the formation of a stable solid shell at the interface increased with decrease in the mold wall thickness and increase in the casting thickness.
- The use of graphite coating on the inner surface of the mold increased the peak heat flux by about 20%.

References

1. H. Huang, O. Gurdogan, H.U. Akay, and W.W. Fincher, Thermal Transport Phenomena in Metal Casting Simulations, *AFS Trans,* Vol 103, 1995, p 243-252
2. M. Jolly, Casting Simulation, How Well do Reality and Virtual Casting Match? State of the Art Review, *Int. J. Cast Met. Res.,* Vol 14, 2002, p 303-313
3. K. Ho and R.D. Pehlke, Metal-Mold Interfacial Heat Transfer, *Metall. Trans. B.,* Vol 16, 1985, p 585-594
4. T.S.P. Kumar and K.N. Prabhu, Heat Flux Transients at the Casting/Chill Interface during Solidification of Aluminum Base Alloys, *Metall. Trans. B.,* Vol 22, 1991, p 717-727
5. J. Campbell, *Castings*, 1st ed., Butterworth-Heinemann, Oxford, UK, 1991, p 125
6. H. Fenech and W.M. Rohsenow, Prediction of Thermal Conductance of Metallic Surfaces in Contact, *J. Heat Transfer,* Vol 85, 1963, p 15-22
7. Y.P. Shlkov and Y.A. Ganin, Thermal Resistance of Metallic Contacts, *Int. J. Heat Transfer,* Vol 7, 1964, p 921-929
8. A.I. Veinik, *Thermodynamics for the Foundryman*, Maclaren, London, UK, 1969, p 1-18
9. J. Isaac, G.P. Reddy, and G.K. Sharma, Variations of Heat Transfer Coefficients during Solidification of Castings in Metallic Molds, *The British Foundryman*, 78, 1985, p 465-468
10. Y. Nishida, W. Droste, and S. Engler, The Air-Gap Formation Process at the Casting-Mold Interface and the Heat Transfer Mechanism through the Air Gap, *Metall. Trans. B.,* 16, 1986, p 833-844
11. D.J. Browne and D. O'Mahoney, Interface Heat Transfer in Investment Casting of Aluminum Alloys, *Metall. Mater. Trans. B.,* Vol 32, 2001, p 3055-3063
12. D.R. Gunasegaram and T.T. Nguyen, Comparison of Heat Transfer Parameters in Two Permanent Molds, *AFS Trans.,* Vol 105, 1997, p 551-556
13. J.S. Kim, M. Isac, R.I.L. Guthrie, and J. Byun, Studies of Interfacial Heat Transfer Resistances and Characterization of Strip Microstructures for Al-Mg Alloys Cast on a Single Belt Casting Simulator, *Canadian Met. Quarterly,* Vol 41 (No. 1), 2002, p 87-96
14. L. Strezov and J. Herbertson, Experimental Studies of Interfacial Heat Transfer and Initial Solidification Pertinent to Strip Casting, *ISIJ Int.,* Vol 38, 1998, p 959-966
15. C.A. Muojekwu, I.V. Samarasekara, and J.K. Brimacombe, Heat Transfer and Microstructure during Early Stages of Metal Solidification, *Metall. Trans. B.,* Vol 26, 1995, p 361-381
16. W.D. Griffiths, The Heat Transfer Coefficient during Unidirectional Solidification of an Aluminum Alloy, *Metall. Mater. Trans B.,* Vol 30, 1991, p 473-482
17. C.P. Hallam, W.D. Griffiths, and N.D. Butler, Interfacial Heat Transfer between a Solidifying Aluminum Alloy and a Coated Die Steel, *Mater. Sci. Forum,* Vol 329-330, 2000, p 467-472
18. J.V. Beck, Nonlinear Estimation Applied to the Nonlinear Heat Conduction Problem, *J. Heat Transfer,* Vol 13, 1970, p 703-716
19. K.N. Prabhu and J. Campbell, Investigation of Casting/Chill Interfacial Heat Transfer during Solidification of Al-11% Si Alloy by Inverse Modeling and Real-Time X-ray Imaging, *Int. J. Cast Metals Res.,* Vol 12, 1999, p 137-143